Improving Photometric Calibration of Meteor Video Camera Systems

Steven Ehlert[a], Aaron Kingery[b], and Robert Suggs[c]

[a]*Qualis Corporation/Jacobs ESSSA Group, NASA Meteoroid Environment Office, Marshall Space Flight Center, Huntsville, AL, USA, 35812*
[b]*ERC/Jacobs ESSSA Group, NASA Meteoroid Environment Office, Marshall Space Flight Center, Huntsville, AL, USA, 35812*
[c]*NASA Meteoroid Environment Office, Marshall Space Flight Center, Huntsville, AL, USA, 35812*

Abstract

We present the results of new calibration tests performed by the NASA Meteoroid Environment Office (MEO) designed to help quantify and minimize systematic uncertainties in meteor photometry from video camera observations. These systematic uncertainties can be categorized by two main sources: an imperfect understanding of the linearity correction for the MEO's Watec 902H2 Ultimate video cameras and uncertainties in meteor magnitudes arising from transformations between the Watec camera's Sony EX-View HAD bandpass and the bandpasses used to determine reference star magnitudes. To address the first point, we have measured the linearity response of the MEO's standard meteor video cameras using two independent laboratory tests on eight cameras. Our empirically determined linearity correction is critical for performing accurate photometry at low camera intensity levels. With regards to the second point, we have calculated synthetic magnitudes in the *EX* bandpass for reference stars. These synthetic magnitudes enable direct calculations of the meteor's photometric flux within the camera band-

pass without requiring any assumptions of its spectral energy distribution. Systematic uncertainties in the synthetic magnitudes of individual reference stars are estimated at ~ 0.20 mag, and are limited by the available spectral information in the reference catalogs. These two improvements allow for zero-points accurate to $\sim 0.05 - 0.10$ mag in both filtered and unfiltered camera observations with no evidence for lingering systematics. These improvements are essential to accurately measuring photometric masses of individual meteors and source mass indexes.
Keywords:
Meteoroids, Photometry, Calibration, Video

---

1. Introduction

Meteor photometry is a fundamental and essential calculation for characterizing individual meteors and meteor showers. Measurements ranging from meteor shower fluxes to the mass of an individual meteor all require accurate measurements of the meteor's radiative emission, usually determined using the techniques developed to measure photometric fluxes of stars in telescopic observations. While this procedure is straightforward in principle, the practical considerations that go into the design of meteor camera systems add complications to the procedure. Many of these complications are rarely considered by meteor observers, which in turn introduces large systematic uncertainties and errors into their photometric measurements.

The first design consideration that greatly impacts the final photometry is an accurate understanding of the camera's response and linearity. Meteor video cameras are commonly set to have a non-linear response, where the

measured signal in the camera ($F_{\rm out}$) is related to the flux of the source ($F_{\rm in}$) via a power-law scaling ($F_{\rm out} = A \times F_{\rm in}^{\gamma}$) in order to increase their contrast and dynamic range. Any errors in mapping the raw camera counts back onto a linear system (hereafter referred to as the linearity correction) will lead to large systematic errors in photometry that depend on the magnitude of the sources in question.

At the same time, meteor cameras are typically not equipped with the same astronomical filters utilized in the observations and determinations of the reference star magnitudes in order to maximize their sensitivity to meteors. A color correction to account for differences between the reference and detector bandpasses therefore must be included. Although the color term for a sample of reference stars can be calculated, that color term is not valid for meteors. Unlike the predominantly thermal/black-body spectral energy distributions (SED's) observed from stars, meteor SED's are typically dominated by emission lines either from its own metals or the atmosphere.

Without careful consideration for the linearity correction and color corrections of the video cameras used to observe meteors, any resultant photometry is potentially subject to large errors. Critically, these errors are highly nonlinear in nature and vary on a meteor-by-meteor basis, which makes it difficult to predict their overall scale from the observational data alone. Given the foundational role meteor photometry plays in characterizing meteor showers subsequent calculations such as the masses of individual meteors or the mass index of a meteor shower may in turn be subject to severe errors.

In this paper, we discuss methods that the NASA Meteoroid Environment Office (MEO) has developed to address these potentially large systematic

errors in meteor photometry. While the precise models we have determined are only directly applicable to the camera systems deployed by the MEO, most of the methodologies and tests discussed below can be modified to accommodate the specific hardware and software utilized by other meteor video camera networks.

2. The MEO's All-sky and Wide-field Camera Networks

The MEO has two video networks which observe meteors nightly- the All-sky network and Wide-field network. Both camera networks utilize Watec 902H2 Ultimate charge-coupled device (CCD) cameras set with manual gains. These cameras are equipped with Sony EX-View HAD ICX429ALL CCD chips. The cameras deliberately set the γ parameter to the "LO" setting on the back of the camera and subsequently have a non-linear response that should correspond to $\gamma = 0.45$ based on manufacturer specifications.

Each of the All-sky cameras is equipped with a 2 mm $f/1.4$ fisheye lens. Half of the Wide-field cameras are outfitted with 17 mm $f/0.95$ Schneider XENON lenses and the other half use 17 mm $f/0.95$ Navitar lenses, producing a $22^\circ \times 16^\circ$ field of view. The video signal is read in through video capture cards on Linux computers using the `ASGARD` meteor detection software (Weryk et al., 2008; Brown et al., 2010). The camera data is read into computers using Brooktree or Sensoray 810 video capture cards. For both camera networks the cameras run at 30 frames per second. The nominal limiting mass for meteors detected in the All-sky camera network is $\sim 1\,\mathrm{g}$, corresponding to a meteoroid sizes of $\sim 1\,\mathrm{cm}$. The Wide-field network has a nominal limiting mass of $\sim 10^{-3}\,\mathrm{g}$, corresponding to grain sizes of $\sim 1\,\mathrm{mm}$.

In addition to the unfiltered camera systems, the MEO deployed a series of four photometric color cameras in June of 2015. These four Watec 902H2 Ultimate CCD video cameras are equipped with 17 mm $f/0.95$ focal length Navitar lenses, giving them an identical field of view as the Wide-field cameras. Each of these cameras is equipped with different standard Johnson-Cousins astronomical filters ($BVRI$) to provide photometric color measurements of meteors. These four cameras work in tandem with the signal from one of the unfiltered Wide-field cameras, and record data in each of the four filters whenever `ASGARD` flags a detection in the unfiltered video feed regardless of the signal present in the color camera data themselves. The need to determine accurate photometric colors of meteors was one of the major drivers behind the MEO's effort to improve their camera calibration procedure.

3. The Scale of Calibration Uncertainties

Before discussing the results of the MEO's laboratory tests, it is important to discuss the level to which the current calibration paradigm is uncertain. We demonstrate this with a simple zero-point calibration model using reference stars observed in a single All-sky event, the data from which is shown in Figure 1. By default, `ASGARD` assumes the response follows a single power-law with $\gamma = 0.45$ across the entire dynamic range and uses R-band reference magnitudes from the SAO J2000 V4 catalog (Myers et al., 2001) to determine the calibration model.

As can be seen in these data, there is a clear segregation between the redder spectral types (e.g. K and M) and the bluer types (e.g. B and A).

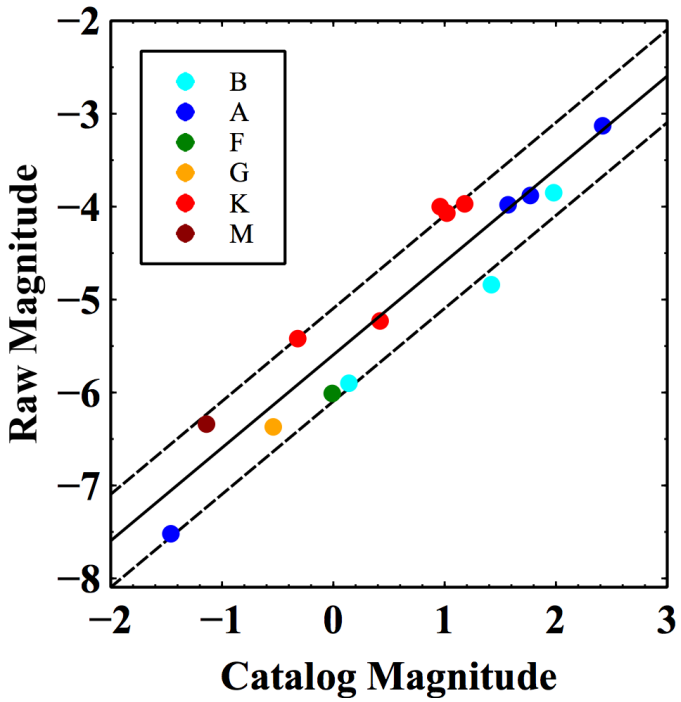

Figure 1: A zero-point calibration model for an All-sky camera observation that demonstrates the level of systematic uncertainty associated with the color correction. The raw magnitudes (y-axis) are taken in an unfiltered camera, whereas the reference magnitudes (x-axis) are derived from the *R*-band using the SAO J2000 V4 catalog. The different colors denote different spectral types. The solid line denotes the best-fit zero-point to all fourteen reference stars, while the dashed lines denote ±0.5 mag around that model.

It is clear that redder stars (types K and M) and bluer stars (types B, and A) have significantly different zero-points than each other as well as average across all spectral types. This uncertainty amounts to ~ 0.5 mag in the zero-point across all stellar spectral types. Critically, this ~ 0.5 mag of uncertainty must be added in quadrature to every source observed in these video data, including the meteor. This uncertainty in the zero-point corresponds to a minimum of $\sim 45\%$ uncertainty in all radiometric measurements derived from photometry. The fractional uncertainty on the meteor mass is equivalent to the fractional uncertainty in the radiometric measurements for an assumed luminous efficiency model and therefore exceeds $\sim 50\%$ for even the brightest meteors. This uncertainty estimate does not account for the expected statistical fluctuations in the aperture photometry/photon counts, which can dominate the uncertainty budget for low signal-to-noise sources. It therefore constitutes a lower limit to the total uncertainty in the luminosity (and subsequently mass) of any meteor detected in our cameras.

Because the photometric color of the meteor in question can vary significantly from the stellar SED's and is frequently unmeasured, systematic errors in the meteor's photometry may still persist even after attempting to account for this uncertainty using reference stars. Even more troubling, these types of systematic errors may consistently overestimate or underestimate meteor masses. An inappropriate linearity correction can be an even larger source of uncertainty than the color term, because it scales with the level of illumination of the camera. Comparing the same meteor observed in two different cameras (with or without filters) could be subject to systematic offsets, as could observations of a single meteor at different times. These

types of errors could greatly skew the distribution of measured magnitudes for a sample of meteors and subsequently affect measurements of the source population index or mass index.

4. Linearity Correction

We performed tests of the camera linearity using two different experiments: one set used observations of a professional-grade chip chart in the Video Calibration Laboratory located at Marshall Space Flight Center. The other set of experiments utilized an inexpensive setup consisting of an Arduino Uno programmable computer board and an off-the-shelf Light-Emitting Diode (LED). Because the LED tests are inexpensive ($\sim$ \$100 US of total equipment) and can be readily reproduced by other meteor camera networks, we will focus on those tests in this work.

The Arduino board was programmed to increase the duty cycle of the LED in 256 equal increments using pulse width modulation, which provides a repeatable standard light-source for which the performance of multiple cameras (or settings on an individual camera) can be directly compared. The LED's brightness levels spanned the full dynamic range of the Watec cameras, and the hardware and software utilized by our test camera system was identical to the deployed systems that are currently taking observations. The linearity correction model was determined for eight Watec cameras in order to quantify variance in the camera-to-camera response.

The results of the LED tests for all eight cameras are shown in Figure 2. All of the cameras show consistent behavior of a linear response at low illuminations and a power-law response at higher intensities. Variations in each

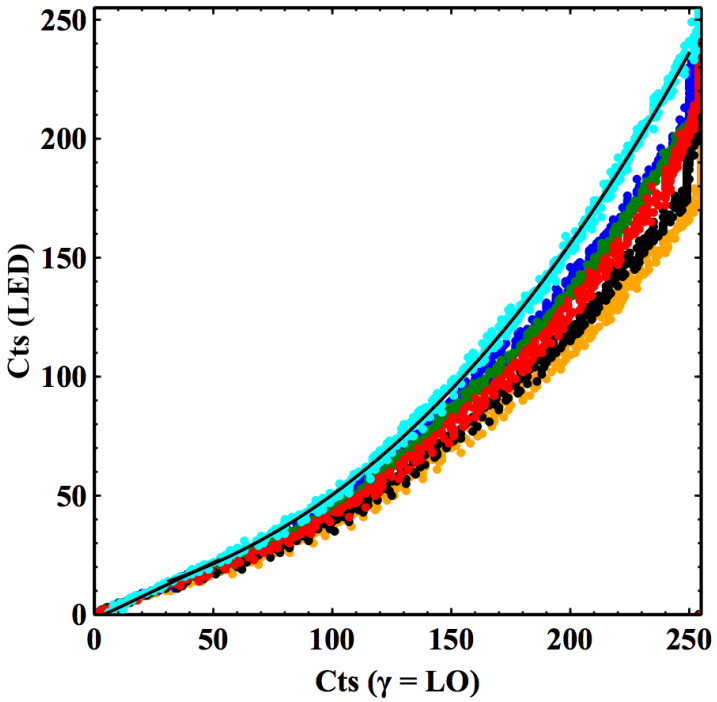

Figure 2: The uncorrected response of eight Watec cameras in the LED test. The x-axis shows the median pixel value within an aperture centered on the LED, and the y-axis is the relative intensity of the LED normalized to a maximum value 256. Each of the eight colors denotes a different camera. The solid black curve denotes the best fit affine + power-law fit to the cyan data points.

camera's gain account for the differences in the overall scaling and saturation limits of each curve. The transition between the affine and power-law components occurs at 30 counts in the uncorrected pixel values, corresponding to $\sim 10\%$ of the maximum pixel values. The power-law index is consistent with $\gamma = 0.45$, and the transition between these two functions occurs at pixel values of ~ 30 in the uncorrected data. Our fiducial linearity correction model is derived from the best-fit model to one of the eight cameras and takes the following parameter values

$$F'(F) = \begin{cases} 2.81 + 0.48 \times F & \text{if } F \leq 30 \\ 255 \times \left(\frac{F+83.19}{370.89}\right)^{1/0.43} & \text{if } F > 30 \end{cases} \quad (1)$$

where F' corresponds to the linearized number of counts in the camera and F denotes the counts in the raw image data. Applying this formula to the data from Figure 2 confirms that the transformed output of each of the eight cameras is linear, which ensures that this single formula can be applied to multiple cameras.

5. A Synthetic Reference Catalog

In order to circumvent the need for a potentially large and highly uncertain correction for the meteor magnitude from the detection bandpass into the reference star's bandpass, we instead determine synthetic magnitudes for all reference stars in the EX bandpass (hereafter the EX-band)[1]. In general,

[1]We name this bandpass after the Sony EX-View HAD CCD chip. The CCD chip is the primary driver of the camera's spectral response, and this particular CCD is utilized by other cameras than the Watec cameras tested in this work.

the observed magnitude of an astronomical source as observed on a photon counting device such as a CCD camera (M) with an arbitrary bandpass is defined as

$$M = -2.5 \log_{10} \left(\frac{\int \lambda \times F_\lambda \times T(\lambda) d\lambda}{\int \lambda \times F_{\lambda,\text{standard}} \times T(\lambda) d\lambda} \right) \tag{2}$$

where F_λ and $F_{\lambda,\text{standard}}$ are the SED's of the source in question and standard source (in units of $\text{erg}\,\text{cm}^{-2}\,\text{s}^{-1}\mathring{A}^{-1}$), λ is the wavelength of light, and $T(\lambda)$ is the wavelength-dependent throughput of the detector[2]. Three model/data components are therefore required to calculate synthetic magnitudes of a source: the wavelength dependent throughput of the detector (hereafter the bandpass); the SED of the source in question; and the SED of a standard source against which all magnitudes are normalized. In order to produce a new reference catalog with calibrated synthetic magnitudes in an arbitrary bandpass we finally require a reference catalog where each source has a calibrated magnitude in a known bandpass.

The EX-band was determined as the product of the quantum efficiency of the Watec's Sony EX-View HAD CCD chip (provided by the manufacturer), the wavelength-dependent transmission of the Navitar lens (also provided by the manufacturer), and the wavelength-dependent transmission of the atmosphere from Capak (2015). The assumed bandpasses for the $BVRI$ filters account for all three of these components as well as the bandpass of the

[2]We emphasize that the initial factor of λ is specifically included for CCD detectors in order to put the integrand into overall units of photon counts. For a photomultiplier tube or calorimeter this additional factor of λ would not be present, since the signal in those detectors depends on the integrated energy of the photons and not the number of photons.

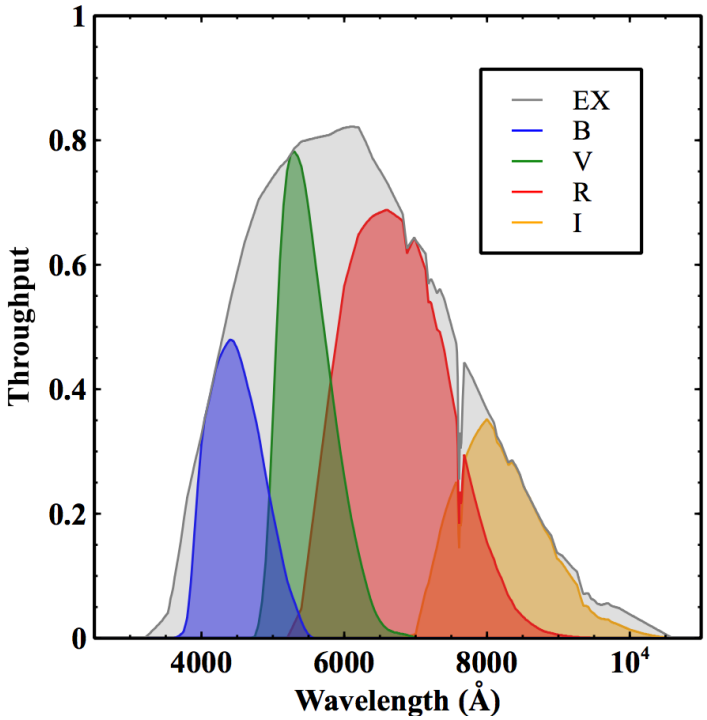

Figure 3: The assumed bandpasses for the unfiltered and color video cameras utilized by the MEO. The color bandpasses further include the transmission efficiency of their respective filters. The dips in throughput red-ward of the EX-band peak correspond to atmospheric absorption lines.

filter itself using the standard Johnson bandpasses included in the `PySynPhot` software package developed by the Space Telescope Science Institute (Lim et al., 2015). All five resultant bandpasses are shown in Figure 3.

We combine our model of the EX-bandpass with the V-band magnitudes and spectral type information from the SAO J2000 V5 Catalog (Myers et al., 2015) to calculate model EX-band magnitudes for each of $\sim 300,000$ of the brightest stars in the sky. We utilize the Morgan-Keenan spectral types

from this catalog (column 'SpMK') whenever possible, as these spectral types include the luminosity class in the spectral type for those stars[3]. Spectral types without the luminosity class are identified for the rest of the stars in the column 'Sp'. Roughly 40% ($\sim$ 120,000 out of 300,000) of the stars in SAO J2000 V5 have the more informative Morgan-Keenan spectral types. Synthetic $EX - V$ colors were determined for each spectral type using the PySynPhot software package (Lim et al., 2015) and the theoretical stellar atmosphere models of Gunn and Stryker (1983); Jacoby et al. (1984); Pickles (1998) included with PySynPhot corresponding to different spectral types and luminosity classes. We have also utilized the unpublished atlases of Bruzal and Bruzal-Persson-Gunn-Stryker included with PySynPhot to maximize the sample of spectral types for which we can determine synthetic magnitudes. All of the synthetic magnitudes and colors were normalized to the SED of Vega in every bandpass.

Synthetic magnitudes were calculated for each source in the SAO J2000 V5 catalog by identifying all model colors whose spectral type included the spectral type of each star. For those stars without a Morgan-Keenan spectral type (e.g. "G2" instead of "G2V") this would include all available luminosity classes. The median color correction across all matching model colors was determined and applied to the reference star's V-band magnitude to determine its model magnitude in all of the other filters. Stars with unusual spectral types such as carbon stars, white dwarfs, or close binaries were not included in these calculations. We supplemented the SAO J2000 V5 Catalog

[3]As an example, the Morgan-Keenan spectral type of a Sun-like star would be "G2V" instead of simply "G2", where the "V" denotes the main-sequence luminosity class.

in a nearly identical manner for stars without measured photometric B, R, or I-band magnitudes in order to ensure that the reference catalog was uniform across all five filters. Actual measurements superseded any magnitudes determined using synthetic colors whenever available.

By doing these calculations in `PySynPhot` we are able to determine the absolute photometric flux of Vega in all five bandpasses, and our zero-point in the EX-band corresponds to a flux of $1.2 \times 10^{-5}\,\mathrm{erg\,cm^{-2}\,s^{-1}}$. Because the CCD cameras utilized for these camera networks are fundamentally photon counting devices, this conversion factor from magnitudes into a physical energy flux depends on the SED of the source in question[4] . As a more precise estimate for this conversion factor for meteors and its expected variance, we have calculated the relative energy per photon for each of the 90 meteor spectra from Vojáček et al. (2015) and compared it to the average energy per photon for Vega. The values of this ratio for these spectra span a range of values from $0.78 - 1.06$ and a median value of 0.93, indicating that the conversion from meteor photometric magnitudes to radiative power is uncertain to the level of $\sim 15\%$ due to the generally unknown SED of the meteor. This distribution further suggests that a $EX = 0$ mag meteor emits $\sim 7\%$ less radiative power than Vega in the EX bandpass on average.

[4]This arises because two sources with identical signals in a CCD camera have the same number of photons detected across the bandpass. The average energy per photon of the two sources can differ based on their individual SED's.

5.1. Testing the Validity of Synthetic Magnitudes Using CCD Observations

The synthetic magnitude procedure we have implemented cannot account for all of the observed and expected variations in stellar spectra, and these modeling deficiencies manifest themselves as systematic/intrinsic scatter in the photometric calibration model. Further tests are required to determine the level of systematic uncertainty this procedure introduces into the final photometric measurements of meteors as well as confirm that no additional measurement biases are present. In order to validate the synthetic magnitudes and estimate the systematic uncertainties associated with this modeling, we utilized observations of the sky with an Andor iKon 936 CCD camera (hereafter the Andor camera) equipped with a Nikon DX 18-55mm f/3.5-5.6GII AF-S Nikkor lens during the peak nights of the Perseid and Geminid meteor showers.

The Andor camera was deployed to observe the sky at a fixed altitude and azimuth continuously over an entire night with repeated 30 s exposures. The focal length of the lens was set to its maximum value of 55 mm, resulting in a field of view of $\sim 30^\circ \times 30^\circ$. In a single 30 s exposure, thousands of stars as faint as ~ 10 mag are detected. Synthetic magnitudes for the Andor bandpass (hereafter the A-band) were determined in the same manner as for the EX-band, albeit with different response curves for both the lens and camera chip. The bandpasses for the Andor and Watec cameras are shown in Figure 4. While the A-band and EX-band bandpasses are not identical in shape, they cover similar wavelength ranges and the peaks of their response curves are at similar wavelengths. These features indicate that trends measured in the A-band can be safely assumed for the EX-band as well.

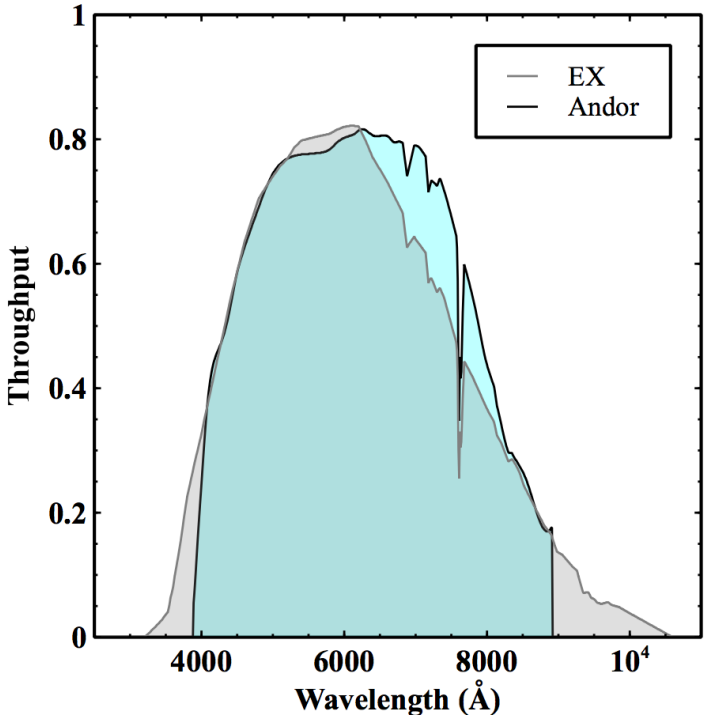

Figure 4: The assumed bandpasses for the Watec (EX, in gray) and Andor (A, cyan) cameras.

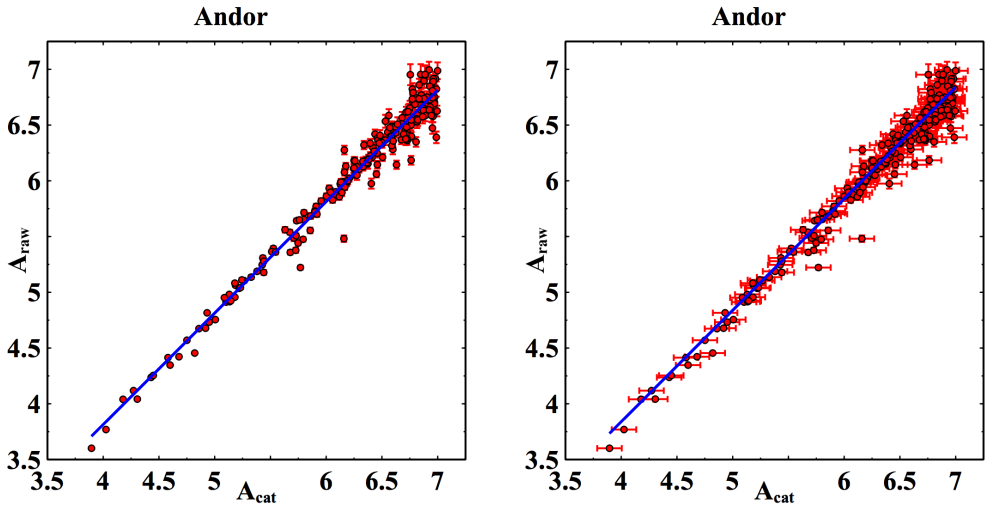

Figure 5: Zero-point figures for an individual 30 s observation of the sky using the Andor camera during the Geminid shower. *Left*: The raw magnitudes versus synthetic Andor-band catalog magnitudes, with the best-fit zero-point model overlaid in red. *Right*: The same data as the left plot with additional systematic uncertainty added to each stellar reference magnitude in quadrature. For this image the systematic uncertainty is estimated at 0.10 mag.

An example zero-point fit of the Andor observation data is shown in Figure 5, and demonstrates that a simple zero-point calibration model with intrinsic scatter is a good descriptor of the data. We estimate the systematic uncertainty associated with our synthetic magnitudes by adding additional uncertainties to the measured uncertainties in quadrature and repeat the zero-point calculation until we reach a reduced χ^2 value of 1. This procedure consistently resulted in a systematic uncertainty of $\sim 0.06 - 0.20$ mag per star. We therefore conservatively add 0.20 mag of systematic uncertainty in quadrature to the measurement uncertainties when performing stellar photometry regardless of the filter.

6. Photometric Performance

We now discuss the overall performance of our new photometric calibration model using unfiltered (EX-band) and filtered observations of a single meteor event. The zero-point determinations for the unfiltered and color video camera systems are shown in Figures 6 and 7, respectively. The error bars in both plots account for uncertainties arising from both the aperture photometry statistics and the systematic uncertainty associated with the bandpass transformation, which are assumed to be 0.20 mag for every reference star based on the results from the Andor observations. Unlike the zero-point model of Figure 1, there exists no evidence of significant color-dependent segregation in the reference magnitudes. In fact, there is no evidence for any intrinsic scatter in either plot not already accounted for by the calculated uncertainties.

The All-sky cameras are able to measure a zero-point with ~ 0.04 mag

precision, the calibration data for which is shown in Figure 6. Critically, there exists no evidence for any intrinsic scatter in these data points not already accounted for in the error bars, which themselves account for the statistical uncertainties in the aperture photometry, with 0.20 mag of systematic uncertainty added in quadrature to address synthetic magnitude modeling deficiencies. The Wide-field calibration data, also shown in Figure 6, is able to measure a zero-point to the same level of precision. Tests of a more sophisticated zero-point + extinction model shows no statistically significant improvement in the fit when adding an airmass-dependent term to the calibration model. As compared to our previous calibration algorithms, the zero-points in the All-sky and Wide-field cameras are offset by ~ 0.5 mag and their statistical uncertainties are approximately a factor of six smaller.

The precision of the zero-points for this event in each filter are 0.10 mag in the B-band, 0.05 mag in the V-band, 0.03 mag in the R-band, and 0.04 mag in the I-band. The reference star data and best-fit zero-point models for each color filter are shown in Figure 7. Again, there exists no evidence in any of the four filters of intrinsic scatter or color dependent segregation in the calibration model, and no statistically significant improvement exists to the calibration model by adding an extinction term.

From the standpoint of meteor masses, a $\sim 0.05 - 0.1$ mag uncertainty in the zero-point corresponds to a $\sim 5 - 9\%$ statistical uncertainty in the meteor's photon flux. We were able to estimate the systematic uncertainty in converting the meteor magnitudes into an energy flux at $\sim 15\%$, which provides a total uncertainty in radiometric measurements (and subsequently meteor masses) at $\sim 16 - 18\%$, at least a factor of two smaller than our

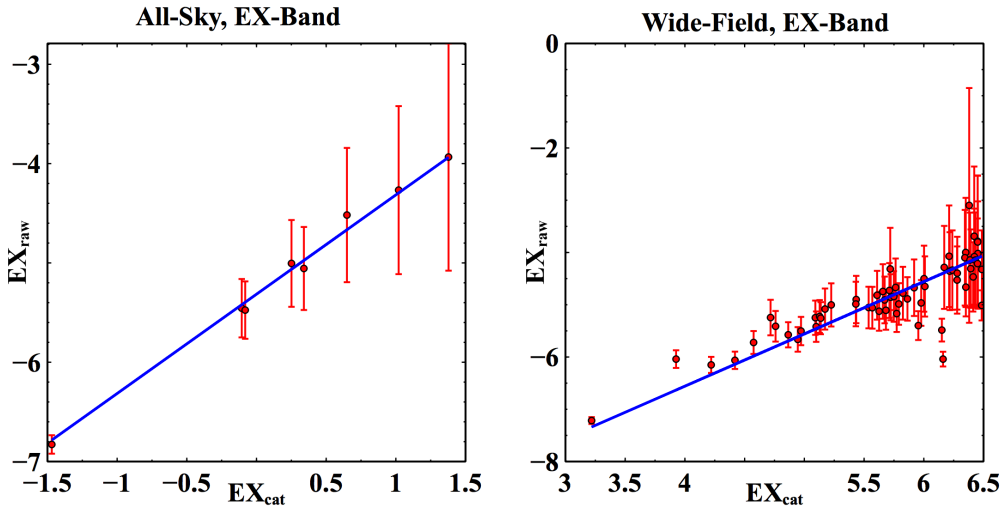

Figure 6: Zero-point calibration models for the unfiltered (EX-band) All-sky and Wide-field cameras. *Left:* The All-sky zero-point calibration model. *Right:* The Wide-field zero-point calibration model. In both sub-figures the raw magnitude is plotted as a function of the catalog magnitude, with the solid line showing the best-fit zero-point calibration model. The slope of the line is fixed to unity.

previous calibration model.

7. Discussion and Future Work

The results of these lab tests demonstrate the importance of testing meteor camera setups in the laboratory prior to deploying them for meteor observations. Without incorporating the new linearity correction and synthetic magnitudes the systematic uncertainties on the zero-point were estimated at ~ 0.5 mag. Applying this calibration model to the meteor itself results in even larger but unquantified systematic uncertainties due to the unknown photometric color of individual meteors as well as errors in the linearity correction being applied to the data. With these corrections in place the

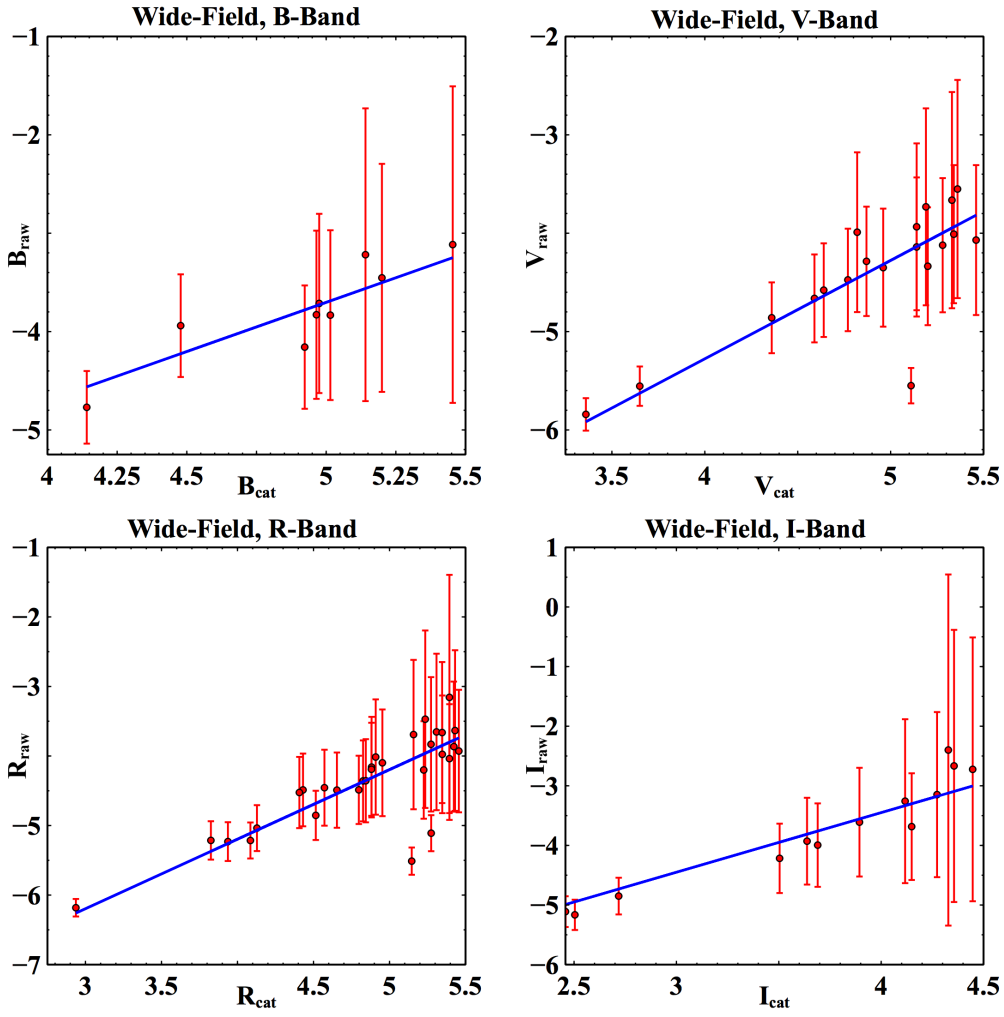

Figure 7: Zero-point calibration models for the filtered color cameras, which have an identical field of view as the Wide-field cameras. In all four sub-figures the raw magnitude is plotted as a function of the catalog magnitude, with the solid line showing the best-fit zero-point calibration model. The slope of the line is always fixed to unity. *Top Left*: The calibration model for the B-band, which has a precision of 0.10 mag. *Top Right*: The calibration model for the V-band, which has a precision of 0.05 mag. *Bottom Left*: The calibration model for the R-band, which has a precision of 0.03 mag. *Bottom Right*: The calibration model for the I-band, which has a precision of 0.04 mag.

statistical uncertainty in the zero-point is reduced to $\lesssim$ 0.10 mag and shows no evidence for further systematic uncertainties.This improvement alone is able to reduce uncertainties in meteor masses from $\sim 50\%$ to $\sim 18\%$ for the exact same camera data. Although the absolute improvement in the zero-point uncertainty is highly significant, the reduction of potential systematic offsets and biases in the measurements ensures that these measurements are not only more precise but also more accurate.

We reiterate that the particular results presented here are specific to the MEO's combination of Watec 902H2 Ultimate video cameras, Sensorary/Brooktree video capture cards, and `ASGARD` meteor detection software. They should not be blindly applied to any other meteor video camera system. The general trends, testing procedures, and algorithms employed by this work are almost certainly applicable to other camera systems, but dedicated tests using systems that replicate deployed cameras as closely as possible are essential to confirming its performance and accuracy. Ideally, this battery of tests (or a variant thereof) is integrated into the commissioning phase of every meteor camera before deployment in order to ensure conformity with manufacturer expectations or to provide the opportunity for camera-specific calibration parameters. The `PySynPhot` package enables synthetic magnitudes to be calculated for an arbitrary bandpass, enabling meteor luminosities to be accurately measured in nearly any camera system whenever its bandpass can be assumed or measured.

While the changes to the MEO's photometry procedure discussed here have greatly improved both the accuracy and precision to which we can measure meteor magnitudes, further development and testing will enable

even better performance. Future surveys and reference catalogs may provide more accurate SED's for the stars observed in the MEO's camera networks. Incorporating future spectroscopic data of reference stars into our procedure will further reduce systematic uncertainties on synthetic magnitudes below the level of ~ 0.20 mag that we have estimated. Finally, the MEO is currently developing and testing methods to correct for saturation in the cameras, which effectively extends the dynamic range of the cameras at the bright end. This development will be especially useful for the All-sky cameras, with saturated events corresponding to bright fireballs likely of public interest.

Acknowledgements

This work was supported by NASA's Meteoroid Environment Office managed by Dr. William Cooke under NASA Contract MSFC-NNM12AA41C (SE and AK). We thank him for his continued support of improving meteor photometry through the tests described in this work. We also thank him for countless discussions regarding the details of this manuscript and the needs of the office. The Meteoroid Environment Office is supported by NASA's Office of Safety and Mission Assurance.

Without the equipment and expertise of other branches at Marshall Space Flight Center, the tests discussed in this work simply would not have been possible. We graciously thank Walt Lindblom for his assistance in our camera linearity measurements, which were performed in the NASA Imagery Experts Program Digital Television Test Facility. Those tests were crucially important in the determination of our final linearity correction. We also wish to thank the Space Telescope Science Institute for their development

and support of the `PySynPhot` synthetic photometry package, which has also been essential in performing the calculations presented here.

We finally thank the anonymous referees for their comments and suggestions, which have improved this manuscript.

Brown, P., Weryk, R. J., Kohut, S., Edwards, W. N., Krzeminski, Z., Feb. 2010. Development of an All-Sky Video Meteor Network in Southern Ontario, Canada The ASGARD System. WGN, Journal of the International Meteor Organization 38, 25–30.

Capak, P., 2015. COSMOS Filters. http://www.astro.caltech.edu/~capak/filters/atm_airmass1.2.cat.

Gunn, J. E., Stryker, L. L., Jun. 1983. Stellar spectrophotometric atlas, wavelengths from 3130 to 10800 A. ApJS52, 121–153.

Jacoby, G. H., Hunter, D. A., Christian, C. A., Oct. 1984. A library of stellar spectra. ApJS56, 257–281.

Lim, P., Diaz, R. I., Laidler, V., 2015. PySynphot User's Guide . STSci Online Guide, http://ssb.stsci.edu/pysynphot/docs/.

Myers, J. R., Sande, C. B., Miller, A. C., Warren, Jr., W. H., Tracewell, D. A., Sep. 2001. VizieR Online Data Catalog: SKY2000 Catalog, Version 4 (Myers+ 2002). VizieR Online Data Catalog 5109.

Myers, J. R., Sande, C. B., Miller, A. C., Warren, Jr., W. H., Tracewell, D. A., Feb. 2015. VizieR Online Data Catalog: SKY2000 Master Catalog, Version 5 (Myers+ 2006). VizieR Online Data Catalog 5145.

Pickles, A. J., Jul. 1998. A Stellar Spectral Flux Library: 1150-25000 Å. PASP110, 863–878.

Vojáček, V., Borovička, J., Koten, P., Spurný, P., Štork, R., Aug. 2015. Catalogue of representative meteor spectra. A&A580, A67.

Weryk, R. J., Brown, P. G., Domokos, A., Edwards, W. N., Krzeminski, Z., Nudds, S. H., Welch, D. L., Jun. 2008. The Southern Ontario All-sky Meteor Camera Network. Earth Moon and Planets 102, 241–246.